Influence of nanoscale structural features on the physical properties of DC reactive magnetron sputtered Zinc Aluminum Oxide (ZAO) thin films for photovoltaic applications

B. RAJESH KUMAR[a,b*], T. SUBBA RAO[b]
[a]*Department of Physics, Sri Venkateswara University, Tirupati-517502, A.P, India*
[b]*Materials Research Lab, Department of Physics, Sri Krishnadevarya University, Anantapur-515003, A.P, India*

Zinc Aluminum Oxide (ZAO) thin films were deposited on glass substrates by DC reactive magnetron sputtering technique. Studies on structural, morphological, electrical and optical properties with different thickness of films are discussed in detail. XRD patterns exhibits ZAO thin films had a diffraction peak corresponding to (0 0 2) preferred orientation with c-axis perpendicular to the substrate surface. The optical band gap of nanostructured ZAO thin films increases with increase of film thickness from 3.41 to 3.51 eV. The carrier concentration of ZAO thin films are in the range of 3.08 x 10^{20} cm^{-3} – 8.12 x 10^{20} cm^{-3}.

(Received April 12, 2012; accepted October 30, 2012)

Keywords: DC magnetron reactive sputtering, ZAO films, Electrical properties, Optical properties

1. Introduction

Transparent conducting oxide (TCO) coatings are essential for solar cell applications since they constitute a fundamental part in the emerging areas of photovoltaic (PV) devices [1]. But beyond its conventional characteristics of light transparency and good electric conductivity, non toxicity, low cost abundance and easy fabrication at an industrial scale are other characteristics to be considered when choosing a TCO electrode for a PV device. Although TCOs have been known and used for quite some time, research on these materials is still very active to improve their characteristics. Doped ZnO is among few metal oxides which can be potentially used as TCO [2]. The advantages of ZnO are the wide band gap of 3.3 eV, low resistivity, high transparency in the visible range, high light trapping characteristics and low preparation costs. ZnO based TCOs are known to be durable in the presence of hydrogen plasma, which is used for the preparation in Si thin films for photovoltaic applications [3]. The n-type dopants used in ZnO are mainly In^{3+}, Al^{3+}, B^{3+}, Ga^{3+} [4-7]. Among all these dopants Al is relatively cheaper, abundant and non toxic material. Hence Zinc Aluminum Oxide (ZAO) thin films can be a prominent low-cost substitute for high cost Tin-doped In_2O_3 films in all TCO applications. Transparent and conductive ZAO films are now being considered for manufacturing transparent electrodes in the flat panel displays, solar cells and organic light emitting diodes due to the large availability and low cost of the material for large area applications.

Various deposition techniques have been employed to prepare ZAO thin films, including molecular beam epitaxy [8-12]. However among these techniques, sputtering offered many more advantages such as high deposition rate at room temperature, no toxic gas emissions, easy to expand to large scale glass substrate, low cost and simple method. In this article we report the investigations on structural, electrical and optical properties of ZAO thin films prepared by DC reactive magnetron sputtering technique. This paper reports the first observation of ZAO thin films sputtered by taking two individual metal targets of Zn and Al.

2. Experimental details

Zinc Aluminum Oxide (ZAO) thin films were prepared by DC reactive magnetron sputtering technique. High purity of Zinc (99.999%) and Aluminum (99.99%) targets with 2 inch diameter and 4 mm thickness are used for deposition on glass substrates. The base pressure in chamber was 3×10^{-6} Torr and the distance between target and substrate were set at 60 mm. The glass substrates were ultrasonically cleaned in acetone and ethanol, rinsed in an ultrasonic bath in deionized water for 15 min, with subsequent drying in an oven before deposition. High purity (99.99%) Ar and O_2 gas was introduced into the chamber and was metered by mass flow controllers for a flow rate fixed at 30 sccm for Ar and 2 sccm for O_2. Deposition was carried out at a working pressure of 3 mTorr after pre-sputtering with argon for 10 min. The

sputtering power was maintained at 105 W during deposition. The depositions were carried out at room temperature with different thickness by varying the deposition time. Film thickness was measured by Talysurf thickness profilometer. The resulting thicknesses of the films are in the range of 230 - 500 nm. X-ray diffraction (XRD) patterns of the films were recorded with the help of Philips (PW 1830) X-ray diffractometer using CuKα radiation. The tube was operated at 30 KV, 20 mA with the scanning speed of 0.03(2θ)/sec. The resistivities of the films (ρ) were measured using the four-point probe method. Surface morphology of the samples has been studied using HITACHI S-3400 Field Emission Scanning Electron Microscope (FESEM) with Energy Dispersive Spectrum (EDS). EDS is carried out for the elemental analysis of prepared thin films. Optical transmittance of the films was recorded as a function of wavelength in the range of 300 – 1200 nm using JASCO Model V-670 UV-Vis-NIR spectrophotometer (Japan).

3. Results and discussion

Fig. 1 shows normalized XRD patterns of ZAO thin films deposited on glass substrates at room temperature with different thickness. All the films show the ZnO (0 0 2) diffraction peak of hexagonal wurtzite structure. It indicates that the films are highly textured with the c-axis orientation in the film growth direction because the c-axis orientation is the most densely packed and thermodynamically favorable one in the wurtzite structure. However the diffraction angle of the (0 0 2) peak shifts towards higher angle side (34.05° - 34.65°).

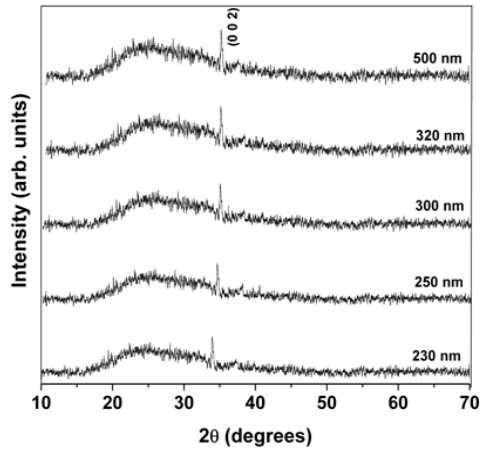

Fig. 1. XRD patterns of ZAO thin films.

The full width at half-maximum (FWHM) can be used to estimate the crystallite size along c-axis, based on the XRD results. The average crystallite size (D) of ZAO thin films prepared with different thickness was calculated using Scherrer's formula

$$D = \frac{0.9\lambda}{\beta \cos\theta} \quad (1)$$

Where λ is the X-ray wavelength (0.154 nm), θ is the Bragg angle, and β is FWHM of (0 0 2) diffraction peak. The average crystallite sizes were in the order of 26 – 46 nm, which indicates that the deposited films are nanostructured. The average crystallite size decreases with the increase of film thickness from 230 to 500 nm.

The lattice constants and the film stress of ZAO thin films are obtained from XRD data. The lattice constant c can be evaluated by the following formula [13]:

$$\frac{1}{d_{hkl}^2} = \frac{4}{3}\left(\frac{h^2+hk+k^2}{a^2}\right) + \frac{l}{c^2} \quad (2)$$

Where a and c are the lattice constants, and d_{hkl} is the crystalline plane distance for indices (h k l). It was found that all d values are larger than that of standard ZnO powder d_o, which is equal to 0.2603 nm. According to equation (2), the lattice constant c is equal to 2d for the (0 0 2) diffraction peak. Compared with the zinc oxide powders [14], all the ZAO thin films in our experiment exhibit discrepancy in d-value, which is due to the variation of residual stress developed in the films. The strain of the films in the direction of c-axis as determined by XRD is $\varepsilon = (c_{film} - c_o)/c_o$, where c_o (= 0.5205 nm) is unstrained lattice parameter measured from ZnO powder. The film stress can be calculated based on the biaxial strain model [15]. The films stress σ_{film} parallel to the films surface can be derived by the following formula, which is valid for a hexagonal lattice [16]:

$$\sigma_{film} = \frac{2c_{13}^2 - c_{33}(c_{11}+c_{12})}{2c_{13}} \times \frac{c_{film}-c_o}{c_o} \quad (3)$$

For the elastic constants c_{ij}, data of single-crystalline ZnO have been used c_{11} = 208.8, c_{33} = 213.8, c_{12} = 119.7, c_{13} = 104.2 GPa. The following numerical relation for the stress derived from XRD can be obtained:

$$\sigma_{film} = -232.8 \times \varepsilon \ (GPa) \quad (4)$$

The negative sign equation (4) corresponds to compressive stress. The residual stress shown in Fig. 2 increases with the increase of film thickness.

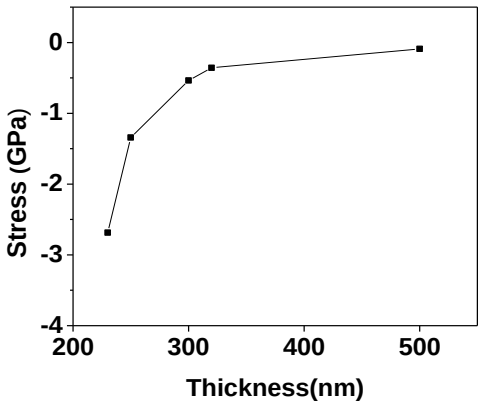

Fig. 2. Variation of film stress as a function of film thickness.

Fig. 3(a) - 3(e) shows scanning electron microscopy (SEM) images of ZAO thin films deposited on glass substrate at different thickness. It is found that grains in SEM images have a geometric form of ellipsoid instead of columnar structure which is usually obtained by sputtering technique. Fig. 4 shows EDS plot with its compositional elemental data for the ZAO thin film of thickness 300 nm.

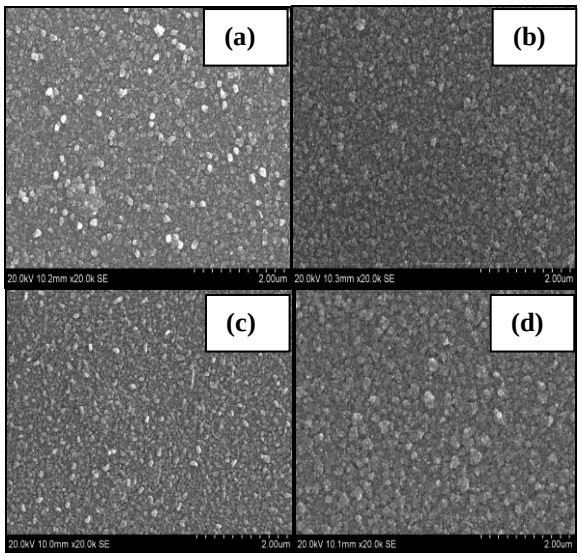

Fig. 3. Surface morphology of ZAO films with thickness of (a) 250 nm, (b) 300 nm, (c) 320 nm, and (d) 500 nm.

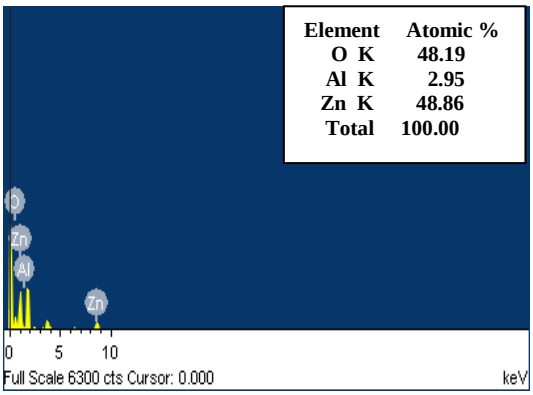

Fig. 4. EDS plot of ZAO film with 300 nm thickness.

AFM images of ZAO thin films shown in Fig. 5 indicate that the films are dense and homogeneous. The surface morphology becomes rougher as film thickness increased. The root-mean-square (rms) surface roughness of ZAO thin films with thickness 250, 300, 320 and 500 nm are 18.61, 18.81, 21.04, 21.32 and 22.62 nm respectively. As the film thickness increases, the root-mean-square (rms) surface roughness of the thin films increases. These film surface morphologies have a potential application in enhanced light trapping particularly in photovoltaic applications.

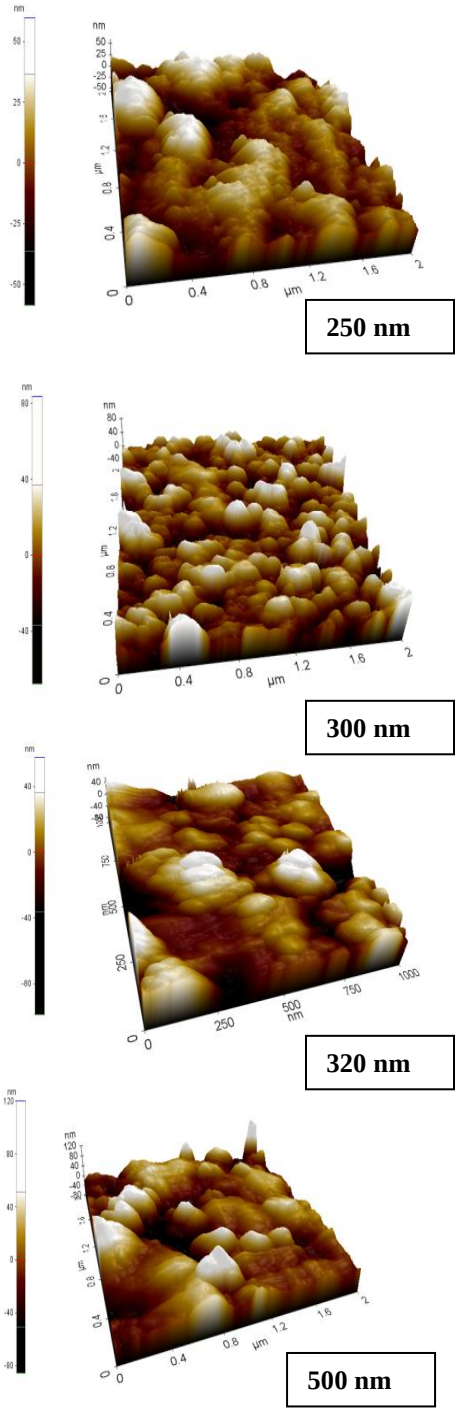

Fig. 5. AFM surface morphology of deposited films with different thickness.

The conduction characteristics of ZAO thin films are primarily dominated by electrons degenerated from Al^{3+} ions substitutional sites of Zn^{2+} ions and Al interstitial atoms. The electrical resistivity (ρ) of the ZAO films was investigated by four-point probe method at room temperature. Fig. 6 shows the variation of the resistivity of ZAO films deposited on glass substrates with different thickness. The increase in film thickness has yielded a reduction in the film's resistivity. The lowest resistivity of

3.44×10^{-4} Ω cm is obtained for the film thickness of 320 nm.

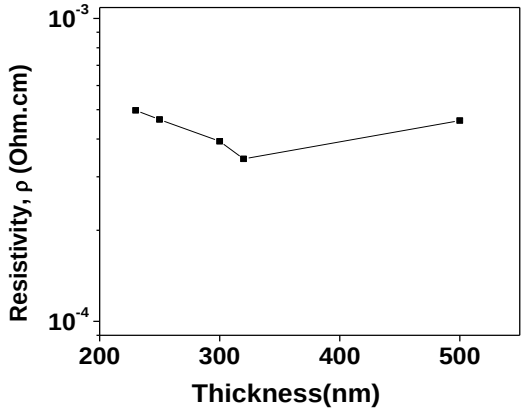

Fig. 6. Variation of resistivity of ZAO films as function of different thickness.

The sheet resistance (R_s) of ZAO thin films is calculated from the equation:

$$R_s = \frac{\rho}{t} \quad \Omega/\square \tag{5}$$

where ρ is resistivity and t is thickness of films. The sheet resistances of ZAO films with thickness of 230, 250, 300, 320 and 500 nm have the values of 21.6, 18.5, 12.1, 10.7 and 9 Ω/□ respectively.

The ZAO film's optical transmittance is shown in Fig. 7. The average visible transmittance for the prepared thin films is > 85%. Due to the thickness effect, it is obvious that the films transmittance decreased as film thickness increased. Thicker films tend to possess multiple internal reflections that occur inside films and as a consequence, it reduces the overall transmittance. It has been known that ZAO film is a direct n-type semiconductor.

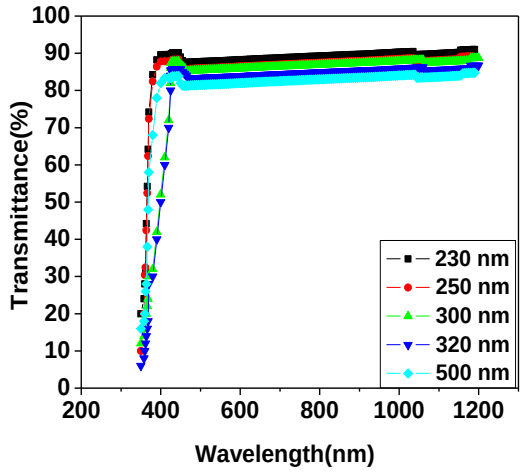

Fig. 7. Optical transmission spectra of ZAO films with different thickness.

The optical band gap of these films is calculated from the transmittance versus wavelength spectra. The absorption coefficient (α) is calculated using the equation [25]

$$\alpha = \frac{\ln\left(\frac{1}{T}\right)}{d} \tag{6}$$

where T is transmittance and d is film thickness. The absorption coefficient (α) and the incident photon energy (hν) is related by the following equation [26]

$$(\alpha h\upsilon)^2 = A(h\upsilon - E_g) \tag{7}$$

where A and E_g are constant and optical band gap, respectively. The E_g can be determined by extrapolations of the linear portion of the curve to hν axis. Fig. 8 shows the curves of $(\alpha h\nu)^2$ versus photon energy. The optical band gap is found varying between 3.41 and 3.51 eV for various films. The optical band gap increases with increase of film thickness shown in Fig. 9. The increase in band gap of ZAO films may be explained by the Burstein-Moss shift.

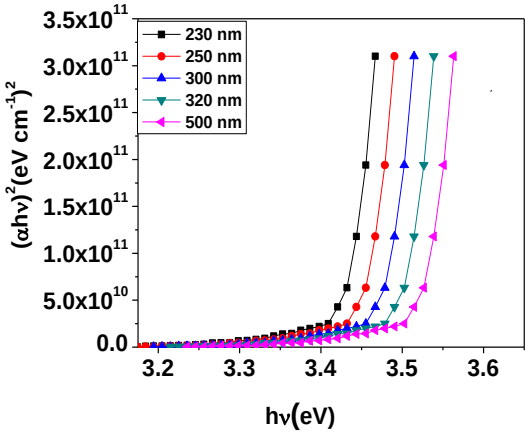

Fig. 8. Plot of $(\alpha h\upsilon)^2$ Vs hυ of ZAO thin films.

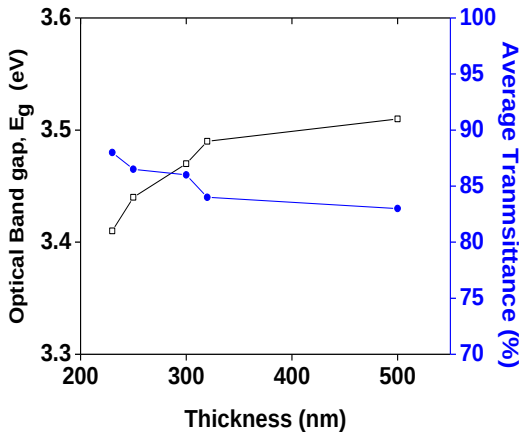

Fig. 9. Variation of optical band gap and average transmittance (in visible region) as a function of film thickness.

The energy band gap widening ΔE_g is related to carrier concentration through the following equation [19]

$$\Delta E_g = \left(\frac{h^2}{8m^*} \right) \left(\frac{3N}{\pi} \right)^{\frac{2}{3}} \quad (8)$$

where h is the Planks constant, m* is the electron effective mass in conduction band, and N is the carrier concentration. From equation (8) it can be found that the energy band gap widening increases with increase in carrier concentration of ZAO thin films. The carrier concentration of ZAO thin films are determined from equation (8) and its is found to be in the range of 3.08×10^{20} cm^{-3} – 8.12×10^{20} cm^{-3}. The carrier concentration increases with increase of thickness.

4. Conclusions

ZAO thin films were prepared on glass substrate by DC reactive magnetron sputtering at room temperature with different thickness. The deposited films are polycrystalline with a hexagonal structure and have a preferred orientation along the c-axis perpendicular to the substrate. The crystallite size, the resistivity and the optical transmittance of the deposited films greatly depend on film thickness. At the optimum thickness of 320 nm, the film has minimum resistivity of 3.44×10^{-4} Ω cm and a high transmittance of above 84% in the visible range. All experimental results indicate that nanostructured ZAO thin films influenced the structural, electrical and optical properties. We achieved ZAO thin films with excellent crystallinity, low resistivity and high transmittance which can be used in photovoltaic devices as front electrode.

Acknowledgements

The authors are thankful to UGC, New Delhi, India for financial support under the major research project (F.NO.37-346/2009, SR).

References

[1] E. Fortunato, D. Ginley, H. Hosono, D. C. Paine, MRS Bull. **32**, 242 (2007).
[2] B.-Y. Oh, M.-C. Jeong, D.-S. Kim,W. Lee, J.-M. Myoung, J. Cryst. Growth **281**, 475 (2005).
[3] H. C. Weller, R. H. Mauch, G. H. Bauer, Sol. Energy Mater. Sol. Cells **27**, 271 (1992).
[4] J. Jie, G. Wang, X. Han, Q. Yu, Y. Lia, G. Li, J. G. Hou, Chem. Phys. Lett. **387**, 466 (2004).
[5] C. David, T. Girardeau, F. Paumier, D. Eyidi, B. Lacroix, N. Papathanasiou, B. P. Tinkham, P. Guérin, M. Marteau, J. Phys: Condens. Matter. **23**, 334209 (2011).
[6] S. Y. Bae, C. W. Na, J. H. Kang, J. Park, J. Phys. Chem. B **109**, 2526 (2005).
[7] A. K. K. Kyaw, X. W. Sun, J. L. Zhao, J. X. Wang, D. W. Zhao, X. F. Wei, X. W. Liu, H. V. Demir, T. Wu, Appl. Phys. **44**, 045102 (2011).
[8] F. K. Shan, Y. S. Yu, J. Eur. Ceram. Soc. **24**, 1869 (2004).
[9] J. Hu, R. G. Gordon, J. Appl. Phys. **71**, 880 (1992).
[10] H. W. Lee, S. P. Lau, Y. G. Wang, K. Y. Tse, H. H. Hng, B. K. Ray, J. Cryst. Growth **268**, 596 (2004).
[11] Eun Soo Jung, Ju Young Lee, Hong Seung, Kim, Nak Won Jang, J. Korean Phys. Soc. **47**, S480 (2005).
[12] Tae Eun Park, Hyung Koun Cho, J. Korean Phys. Soc. **47**, S493 (2005).
[13] G. J. Fang, D. J. Li, B. L. Yao, Phys. Stat. Sol. A **193**, 139 (2002).
[14] H. Kim, A. Pique, J. S. Horwitz, H. Murata, Thin Solid Films **377**, 798 (2000).
[15] A. Segmuller, M. Murakami, R. Roscoberg, Analytical Techniques for Thin Films, Academic Press, Boston, 143 (1988).
[16] R. Cebulla, R. Wendt, K. Ellmer, J. Appl. Phys. **83,** 1087 (1998).
[17] W. Miao, X. Li, Q. Zhang, L. Huang, Z. Zhang, L. Zhang, X. Yan, Thin Solid Films **500**, 70 (2006).
[18] V. R. Shinde, T. P. Gujar, C. D. Lokhande, R. S. Mane, S. H. Han, Mater. Chem. Phys. **96**, 326 (2006).
[19] F. Urbach, Phys. Rev. **92**, 1324 (1953).

[*]Corresponding author: rajphyind@gmail.com